

# LMQFormer: A Laplace-Prior-Guided Mask Query Transformer for Lightweight Snow Removal

Junhong Lin, Nanfeng Jiang, Zhentao Zhang, Weiling Chen, *Member, IEEE* and Tiesong Zhao, *Senior Member, IEEE*

arXiv:2210.04787v1 [cs.CV] 10 Oct 2022

**Abstract**—Snow removal aims to locate snow areas and recover clean images without repairing traces. Unlike the regularity and semitransparency of rain, snow with various patterns and degradations seriously occludes the background. As a result, the state-of-the-art snow removal methods usually retains a large parameter size. In this paper, we propose a lightweight but high-efficient snow removal network called Laplace Mask Query Transformer (LMQFormer). Firstly, we present a Laplace-VQVAE to generate a coarse mask as prior knowledge of snow. Instead of using the mask in dataset, we aim at reducing both the information entropy of snow and the computational cost of recovery. Secondly, we design a Mask Query Transformer (MQFormer) to remove snow with the coarse mask, where we use two parallel encoders and a hybrid decoder to learn extensive snow features under lightweight requirements. Thirdly, we develop a Duplicated Mask Query Attention (DMQA) that converts the coarse mask into a specific number of queries, which constraint the attention areas of MQFormer with reduced parameters. Experimental results in popular datasets have demonstrated the efficiency of our proposed model, which achieves the state-of-the-art snow removal quality with significantly reduced parameters and the lowest running time.

**Index Terms**—Lightweight snow removal, Laplace operator, mask query transformer, image denoising, image enhancement.

## I. INTRODUCTION

**S**NOW seriously affects the visibility of scenes and objects in images. It usually leads to poor visual qualities and severe performance degradations in high-level computer vision tasks such as object detection and semantic understanding. Therefore, the research on snow removal has strong value and significance. However, it is difficult to capture unified patterns in snowy scenes due to their different patterns and transparency. Unlike other types of image noises [1]–[4], snow seriously obscures the background and thus is difficult to be removed. How to recover clean images from snowy scenes is still a challenging issue.

We divide existing snow removal methods into two types: traditional methods and deep-learning-based methods. Traditional methods are based on artificial prior knowledge to

This work was supported in part by the National Natural Science Foundation of China (Grant No. 62171134, 61901119) and in part by Natural Science Foundation of Fujian Province, China (Grant No. 2022J02015, 2022J05117). (Corresponding author: Tiesong Zhao.)

J. Lin, N. Jiang, Z. Zhang and W. Chen are with the Fujian Key Lab for Intelligent Processing and Wireless Transmission of Media Information, College of Physics and Information Engineering, Fuzhou University, Fuzhou 350108, China (E-mails: jhlin\_study@163.com, jnrock@gmail.com, 211120091@fzu.edu.cn, weiling.chen@fzu.edu.cn).

T. Zhao is with the Fujian Key Lab for Intelligent Processing and Wireless Transmission of Media Information, College of Physics and Information Engineering, Fuzhou University, Fuzhou 350108, China and also with the Peng Cheng Laboratory, Shenzhen 518055, China (e-mail: t.zhao@fzu.edu.cn).

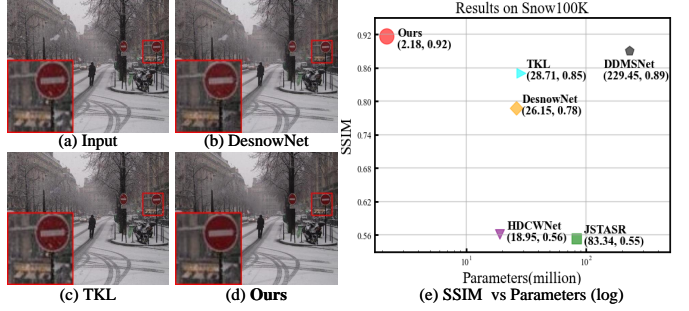


Fig. 1. Our proposed method achieves the state-of-the-art snow removal quality with the lowest computational complexity. (a) A typical real-world snowy. (b)-(d) the outputs of our method and its peers. (e) the performances and parameter sizes of different methods under Snow100K.

model snowy layers, such as HOG and MoG model [5], dictionary learning [6], color assumptions [7] and Hamiltonian quaternions [8]. Deep-learning-based methods take advantages of deep neural networks to remove undesired snow in images, such as DesnowNet [9], CGANs [10], JSTASR [11], HDCWNet [12] and DDMSNet [13].

Despite these great efforts, there are still critical issues to be further addressed. The existing works usually retain a large number of parameter size for better visual qualities, but inevitably, their computational workloads are also remarkably increased. This fact limits their applications in real-world scenarios. Besides, the repairing traces still remain in their results, as shown in the red traffic sign of Fig. 1(b)(c). Therefore, it is essential to design a lightweight but high-efficient network for this task.

It should be noted that the existing rain removal methods cannot well address the snow problem due to the apparent visual differences between rain and snow. As can be seen in Fig. 2(a), the rain drops and streaks are densely distributed while the snowflakes vary in patterns. The image backgrounds are also more sensible for rainy images. The backgrounds of snowy images seriously obscured with different obscuration degrees even in the same scene. These differences make it difficult to use existing rain removal methods (e.g. [14], [15]) or lightweight methods (e.g. [16], [17]) to process snowy images. How to locate snow areas and recover clean images are still important challenges in snow removal.

To solve the above problems, we explore a prior of coarse mask and propose a lightweight architecture called Laplace-prior-guided Mask Query Transformer (LMQFormer). Our main concept of lightweight is to learn vast snow features at

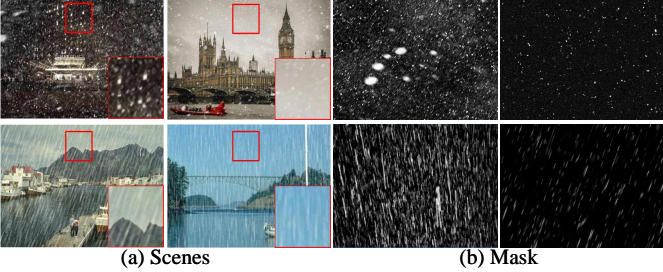


Fig. 2. Examples of snowy and rainy images. (a) typical snowy and rainy scenes [9], [18]. (b) typical snowy and rainy masks [9], [19].

low scales and use coarse mask as prior knowledge to guide the recovery process. On the basis of this, we introduce Laplace operator to remove redundant information while preserving high-frequency snow edge information. A Laplace-VQVAE (Vector Quantised Variational AutoEncoder) is thus formulated to generate the coarse mask as prior knowledge for snow removal. Furthermore, we design a lightweight sub-network called Mask Query Transformer (MQFormer) to use the coarse mask to recover clean images. We employ an efficient framework consisting of parallel transformer and convolutional encoders and a hybrid decoder to learn snow characteristics under lightweight requirements. Duplicated Mask Query Attention (DMQA) is designed to integrate the coarse mask and concentrate the MQFormer to snow areas.

The suggested lightweight design enables our LMQFormer to attain state-of-the-art performance and the fastest processing, as demonstrated in Fig. 1(e). Additionally, our method has better generalization performance on the real-world images, as illustrated in Fig. 1(d). The main contributions are summarized as follows:

- We propose a Laplace-VQVAE to generate a coarse mask as prior of snow areas. The effectiveness and low entropy with Laplace Prior are analyzed and inspire us to design a lightweight snow removal network without training on masks.
- We design an MQFormer to recover clean images under diversified snow patterns. The extensive snow features are learned and processed with an efficient framework consisting of parallel transformer and convolutional encoders and a hybrid decoder. A DMQA network is also developed to concentrate on snow areas during processing.
- We propose an overall LMQFormer network for lightweight snow removal. Our LMQFormer achieves the state-of-the-art quality in popular snow removal datasets with the fastest processing speed and robust generalization performance.

## II. RELATED WORK

### A. Traditional Snow Removal Methods

Prior knowledge has been used to guide traditional methods to recover snowy images. Bossu *et al.* [8] employed MoG model to separate the foreground and used HOG features to detect snow from foreground and recover clean images. Wang *et al.* [6] combined image decomposition with dictionary

learning to model a three-layer hierarchical snow removal scheme. Zheng *et al.* [20] exploited the difference between snow and background and used the multi-guided filter to remove snow. Pei *et al.* [7] extracted snow features on saturation and visibility in HSV color space to detect snow areas for removal. Rajderkar *et al.* [21] applied bilateral filter to decompose snowy image into low frequency and high frequency parts. Then decomposed the high frequency part into snowy foreground and clean background by performing dictionary learning and sparse coding to help snow removal. Voronin *et al.* [5] employed the anisotropic gradients of Hamiltonian quaternions to detect snow areas and recover clean images. Although these methods have certain effects, they only modeled some specific characteristics of snow, which led to poor generalization ability in real-world scenarios.

### B. Deep-learning-based Snow Removal Methods

Recently, deep learning has been successfully applied in single image snow removal task. Liu *et al.* [9] proposed the first deep-learning-based method called DesnowNet. They applied a two-stage network to learn the mapping from snowy images to mask and recover clean images. Li *et al.* [10] used Generative Adversarial Network (GAN) to recover clean images. Chen *et al.* [11] proposed a JSTAR model to generate three different snow masks with differentiable dark channel prior layer and guide image recovery with these masks. Li *et al.* [22] created architectural search and proposed all-in-one network for snow, rain and fog removal. Chen *et al.* [12] proposed HDCWNet, which removed snow with hierarchical dual-tree complex wavelet representation and contradict channel loss. Zhang *et al.* [13] introduced semantic and geometric images as prior knowledge to guide snow removal. Chen *et al.* [23] used a two-stage knowledge distillation learning to recover all bad-weather images, which is called TKL in this paper. In summary, these methods achieve promising performances in snow removal but at costs of large parameter sizes. Besides, their recovered images may remain repairing traces, as shown in Fig. 1(b)(c).

Different from these methods, we aim to explore a prior of coarse mask to guide a lightweight but high-efficient network. The proposed model is also generates images with high visual qualities which will be validated in experimental results.

### C. Other Image Denoising Tasks

There are some other image denoising tasks similar to the snow removal task, including rain removal (*e.g.* [24]), haze removal (*e.g.* [2]), low-light enhancement (*e.g.* [25]) and underwater image enhancement (*e.g.* [26]). For example, Zou *et al.* [27] utilized an adaptive pruning scheme to determine the hierarchical sparsity for rain removal. Zhang *et al.* [28] proposed an Enhanced Spatio-Temporal Integration Network (ESTINet) to exploit the spatio-temporal information for rain streak removal. Wu *et al.* [29] proposed a contrastive regularization for haze removal. Wang *et al.* [30] proposed a normalizing flow model for low-light enhancement. Jiang *et al.* [31] exploited the potential of lightweight network that benefits both effectiveness and efficiency for underwater image enhancement.

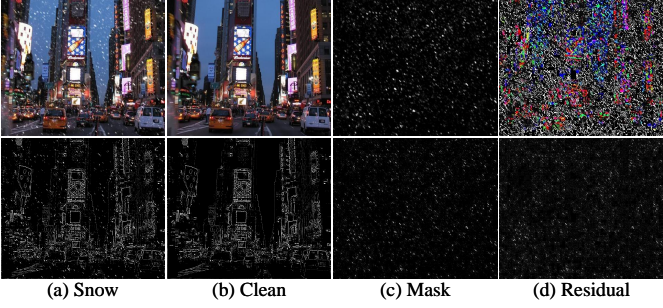


Fig. 3. Snow images processed by Laplace operator. (a) a snowy image before and after being processed by Laplace operator; (b) the clean background images of (a); (c) the snow masks of (a); (d) the residuals calculated by (a)-(b).

### III. METHODOLOGY

#### A. Problem Statement

As discussed in Section II, deep-learning-based snow removal methods take advantage of CNNs to recover clean images. Their deep neural networks learn a mapping from the input snowy image  $I_{\text{snow}}$  and its output  $I_{\text{clean}}$ :

$$I_{\text{clean}} = F_m(I_{\text{snow}}; \theta), \quad (1)$$

where  $F_m(\cdot)$  represents a deep neural network for mapping,  $\theta$  represents the parameters of  $F_m(\cdot)$ . Considering the complicated patterns of snowflakes, existing methods tend to employ complicated networks with large parameter sizes. Although they achieve successes in recovering clean images under snow, their parameter volumes limit their use in practice scenarios *e.g.* surveillance, videos, etc. The snow removal task is still calling for an effective model with a low parameter size and a high processing speed.

To address this issue, we revisit the physical model of snowy image as shown in [9]:

$$I_{\text{snow}} = R \odot M + C \odot (1 - M), \quad (2)$$

where  $R$ ,  $C$  and  $M$  are the chromatic aberration map, the latent clean image and the mask image of  $I_{\text{snow}}$ , respectively. This decomposition inspires us to design a mask-based snow removal approach. However, the snow mask is not available in practical use. Instead, we interpret a coarse mask and further utilize it to form a unified prior that benefits both snow location and removal. This task is thus defined as:

$$\begin{aligned} I_{\text{prior}} &= G_n(I_{\text{snow}}; \theta_A), \\ I_{\text{clean}} &= I_{\text{snow}} - F_n(I_{\text{snow}}, I_{\text{prior}}; \theta_B), \end{aligned} \quad (3)$$

where  $I_{\text{prior}}$  represents this unified prior.  $G_n(\cdot)$  and  $F_n(\cdot)$  represent the sub-networks to generate  $I_{\text{prior}}$  and recover clean images with  $I_{\text{snow}}$  and  $I_{\text{prior}}$ , respectively.

Based on the above analyses, we attempt to construct a unified prior of snow via an interpreted coarse mask and further utilize it in recovering clean images. As shown in Eq. (3), the functions of our prior are twofold. First, it is utilized to coarsely locate snow areas. Second, it is combined with  $I_{\text{snow}}$  to estimate the residuals between the input and output of our model. With a guidance of this prior, we can achieve better snow removal results under the lightweight requirement.

#### B. Laplace Prior

This paper calculates the  $I_{\text{prior}}$  with the sub-network  $G_n(\cdot)$  and the Laplace operator. It is commonly known that lower entropy of data makes ease of the feature extraction of neural network, that is, the network is easier to learn the latent rules of data. Here we define an optimization of the relative entropy of  $I_{\text{prior}}$  and  $I_{\text{snow}}$ :

$$\min_{q_\theta} D_{KL}(q_\theta(I_{\text{prior}} | I_{\text{snow}}) \| p(I_{\text{prior}}))$$

$$s.t. \quad I_{\text{prior}} \sim q_\theta(I_{\text{prior}} | I_{\text{snow}}) \iff I_{\text{prior}} = G_n(I_{\text{snow}}; \theta_A), \quad (4)$$

where  $p(I_{\text{prior}})$  and  $q_\theta(I_{\text{prior}} | I_{\text{snow}})$  represent the prior and posterior probabilities of  $I_{\text{prior}}$ , respectively. This minimization process can help to design the network  $G_n(\cdot)$  and its learning parameters  $\theta_A$ .

In the designing of network  $G_n(\cdot)$ , we amplify the snow features and eliminate the irrelevant information to reduce  $D_{KL}$ . This can be achieved with Laplace operator:

$$I_{\text{lapsnow}} = \nabla^2 I_{\text{snow}}, \quad (5)$$

Correspondingly, the clean image  $I_{\text{clean}}$  outputs  $I_{\text{lapclean}}$  after Laplace operator. From Fig. 3, it is extremely easy to distinguish  $I_{\text{snow}} - I_{\text{clean}}$  (*i.e.* the fourth image in the first row) and the snow mask (*i.e.* the third image in the first row). However, after being processed by Laplace operator, the corresponding images in the second row are quite similar, that is, their differences are negligible. Thus, we are allowed to use  $I_{\text{lapsnow}} - I_{\text{lapclean}}$  as a coarse mask for snow removal.

With Laplace operator, the subnetwork  $G_n(I_{\text{snow}}, \theta_A)$  is replaced by  $G_L(I_{\text{lapsnow}}, \theta_A)$ . Its training process can be expressed as:

$$\min_{G_L(\cdot)} \|G_L(I_{\text{snow}}; \theta_A) - (I_{\text{lapsnow}} - I_{\text{lapclean}})\|_2, \quad (6)$$

where we attempt to train a Laplace prior to approximate the coarse mask without explicit knowledge of  $I_{\text{clean}}$  or  $I_{\text{lapclean}}$ .

#### C. Lightweight Design

With Laplace operator, we can approximate the coarse mask as a prior, as shown in Eqs. 3 and 6 and further utilize it to guide the recovery process, as shown in Eq. 3. This operation allows us to compute more efficiently with low entropy data. The complete model is designed as a lightweight network, which is benefitted from the following modules. First, we introduce spatial attention and Codebook [32] for  $G_L(\cdot)$  to effectively extract spatial features for the coarse mask. Second, we introduce Mask Query Transformer Module (MQTM) to make  $F_n(\cdot)$  concentrate on snow areas, thus, we call our recovery network as  $F_{\text{MQ}}(\cdot)$ . Third, we design an efficient framework consisting of parallel transformer and convolutional encoders and a hybrid decoder to obtain more representative features of snow at low scales. This framework greatly reduce computational workloads while remaining high-performance. By considering all these issues, our complete network is designed as:

$$I_{\text{clean}} = I_{\text{snow}} - F_{\text{MQ}}(I_{\text{snow}}, G_L(I_{\text{snow}}; \theta_A); \theta_B), \quad (7)$$

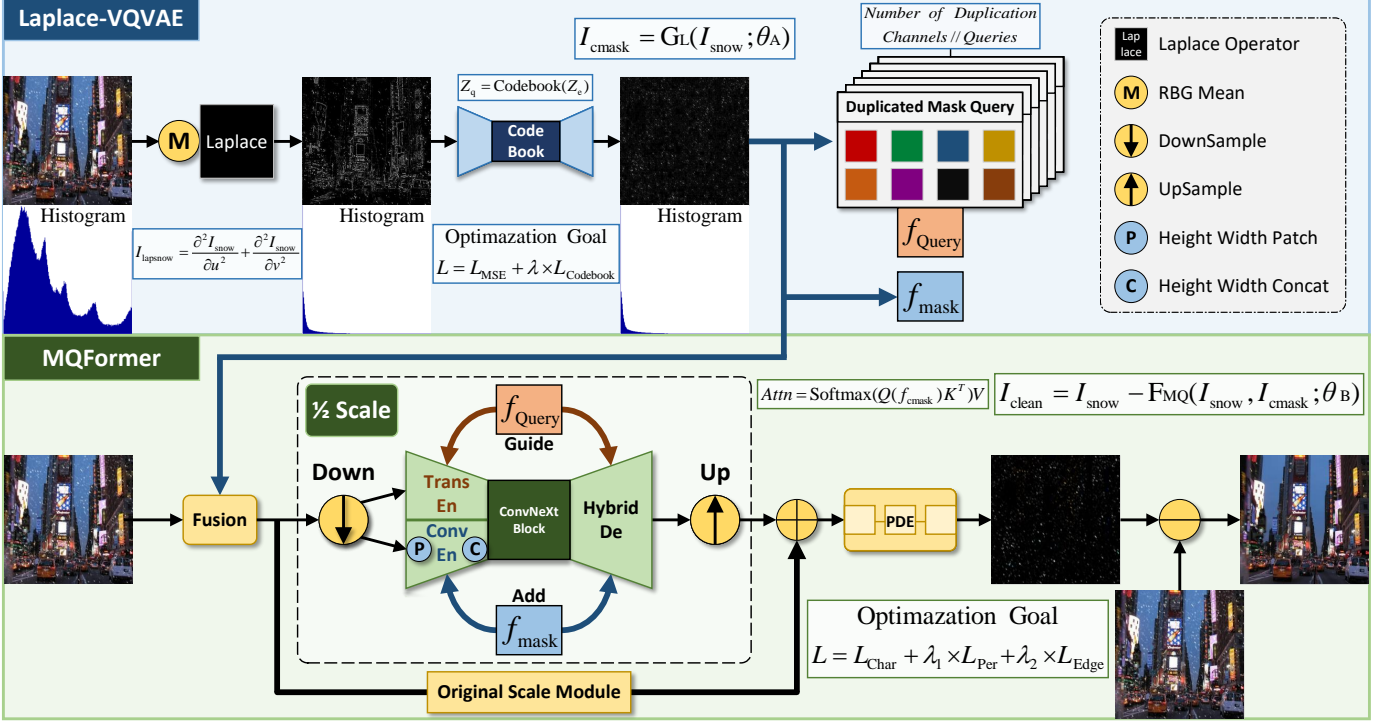


Fig. 4. The overall structure of LMQFormer. As shown in the histogram, we use Laplace operator to reduce the entropy of information in the picture. Further, we design DMQA to guide network pay concentrate attention to snow areas. Due to Laplace prior, our network is lightweight but high-efficient.

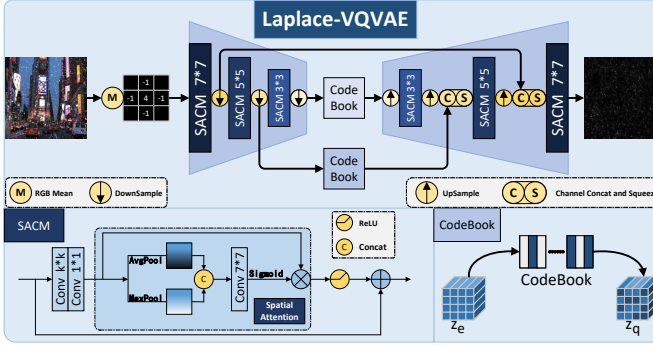


Fig. 5. Laplace-VQVAE. It consists of three layers downsample and Spatial Attention Convolution Module (SACM). Note that from the first to the third layer, the kernel sizes are 7, 5 and 3, respectively.

where  $G_L(\cdot)$  and  $F_{MQ}(\cdot)$  represent the coarse mask generator and the recovery network, respectively.

Based on above analysis, our main concept of lightweight design is to use the coarse mask to guide the recovery process and do most of operations at low scales. Firstly, we introduce spatial attention based module and Codebook [32] for  $G_n(\cdot)$  to learn the effective spatial features to generate the coarse mask. Moreover, we highly integrate mask information into  $F_n(\cdot)$  to guide the recovery process. We introduce Mask Query Transformer Module (MQTM) to let  $F_n(\cdot)$  pay concentrate attention to snow areas. Therefore we call our recovery network as  $F_{MQ}(\cdot)$ . Moreover, we design an efficient framework consisting of parallel transformer and convolutional encoders and a hybrid decoder to obtain more representative features of snow at low scales.

## IV. NETWORK DESIGN

### A. Network Framework

In our paper, we realize  $G_L(\cdot)$  and  $F_{MQ}(\cdot)$  by two sub-networks: Laplace-VQVAE and MQFormer. They formulate a complete Laplace-prior-guided Mask Query Transformer (LMQFormer), as shown in Fig. 4. In Laplace-VQVAE, Laplace operator greatly reduces the information entropy of snow images, as shown in histograms. This makes it easy to build a lightweight sub-network to generate the coarse mask. Then a DMQA module is utilized to make network pay more and concentrate attentions to snow areas. In MQFormer, complex module calculations are carried out at low scales. Parallelized encoders and hybrid decoders are designed to learn diversity representation of features. These designs guarantee the effectiveness of our model with reduced parameters.

### B. Laplace-VQVAE

We design a VQVAE-based [32] lightweight sub-network called Laplace-VQVAE to generate the coarse mask. As shown in Fig. 5, RGB channels are averaged to obtain gray images and then filtered by Laplace operator. Moreover, we design three downsample layers to get multi-scale features and Spatial Attention Convolution Module (SACM) to preserve important spatial information of snow. Based on that fact, our Laplace-VQVAE has only 160k parameters with 24 channels.

As for optimizing VQVAE, the original probability distribution becomes into one-hot form with  $K$  dimensions in total, which corresponds to the probability of embedding in the

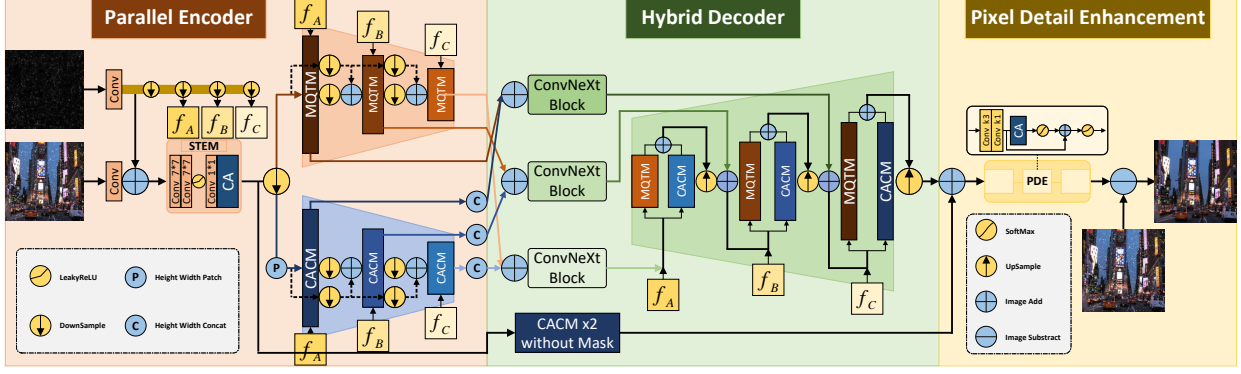


Fig. 6. The details of MQFormer. It consists of transformer encoder, convolutional encoder and hybrid decoder. Hybrid decoder contains all parts of two encoders. The main modules are Mask Query Transformer Module (MQTM) and Channel Attention Convolution Module (CACM).  $f_A$ ,  $f_B$  and  $f_C$  represent stepwise downsamples of the coarse mask features.

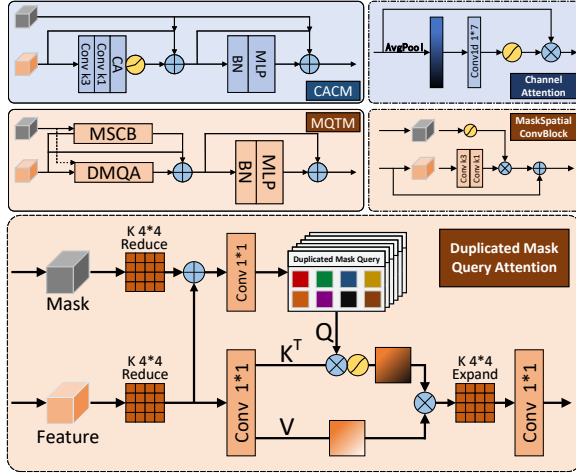


Fig. 7. The details of MQTM and CACM. Mask information is highly integrated with these two modules. MQTM contains Duplicated Mask Query Attention (DMQA). CACM is based on channel attention.

Codebook. Then the KL divergence term in the ELBO of VAE [33] becomes a constant as follows:

$$\begin{aligned} D_{KL}(q(z|x)\|p(z)) \\ = 1 \cdot \log \left( \frac{1}{\frac{1}{K}} \right) + (K-1) \times 0 \cdot \log \left( \frac{0}{\frac{1}{K}} \right) \\ = \log K, \end{aligned} \quad (8)$$

where  $q(z|x)$  represents the probability of the latent code under condition  $x$ ,  $p(z)$  is the prior distribution of the latent code  $z$ . The Codebook optimization goal can be expressed as:

$$\mathcal{L}_{\text{Codebook}}^k = \sum_k^2 \sum_j^{n_i} \|z_{i,j} - e_i\|, \quad (9)$$

where  $k$  represents different layers,  $e_i$  represents vectors in Codebook,  $z_{i,j}$  represents encoded vector. Inspired by VQVAE, we introduce Codebook to enhance the ability to select useful features at low scales.

### C. MQFormer

Fig. 6 shows the details of MQFormer. Due to Laplace prior, our network is lightweight but high-efficient. We design

an efficient framework consisting of two parallel encoders, a hybrid decoder and modified ConvNeXtBlock [34] to learn multi-scale features at low scales. Moreover, Pixel Detail Enhancement (PDE) learn further details on the original scale.

Fig. 7 shows the details of MQTM and CACM, which are the main lightweight components of two parallel encoders and a hybrid decoder. In CACM, the coarse mask prior is directly added to features to prevent information loss. Channel Attention (CA) has only seven parameters due to 1D convolution. We design parallel DMQA and Mask Spatial Convolution Block (MSCB) for MQTM. In DMQA, mask prior is added to Query and then reduced to a specific query number, which is calculated at 1/4 scales through 4×4 kernels. We multiply the mask information directly into MSCB. Besides, MQTM has the same architecture of BatchNorm and MLP as CACM. The formulas of the two branches are as follows:

$$\begin{aligned} f_{\text{MSCB}} &= f_x + \text{Conv}(f_x) \odot \text{Softmax}(f_{\text{cmask}}), \\ K, V &\leftarrow \text{CS}(\text{Conv}_{1*1}(f_x)), \\ Q &\leftarrow \text{CD}(\text{Conv}_{1*1}(f_x + f_{\text{cmask}})), \\ f_{\text{DMQA}} &= \text{Softmax} \left( \frac{QK^T}{\sqrt{d_k}} \right) V, \\ f &= f_{\text{MSCB}} + f_{\text{DMQA}}, \end{aligned} \quad (10)$$

where  $\text{CS}(\cdot)$  represents channel-wise split,  $\text{CD}(\cdot)$  represents channel-wise duplication,  $\text{cmask}$  represents the coarse mask. Since LayerNorm does not contribute to performance and affects the processing speed, we replace it with BatchNorm. We set the ratio of MLP to 4 in MQFormer.

### D. Loss Functions

We separately train Laplace-VQVAE and MQFormer. Laplace-VQVAE is trained by two losses: the squared penalty of Mean Square Error (MSE)  $\mathcal{L}_{\text{MSE}}$  and Codebook Loss  $\mathcal{L}_{\text{Codebook}}$ . The total optimization goal can be expressed as:

$$\mathcal{L}_{\text{Laplace-VQVAE}} = \mathcal{L}_{\text{MSE}} + \lambda * \mathcal{L}_{\text{Codebook}}, \quad (11)$$

where  $\lambda=0.25$  is hyper-parameter of Codebook. MQFormer is trained by three losses: Charbonnier Loss  $\mathcal{L}_{\text{char}}$  [35],

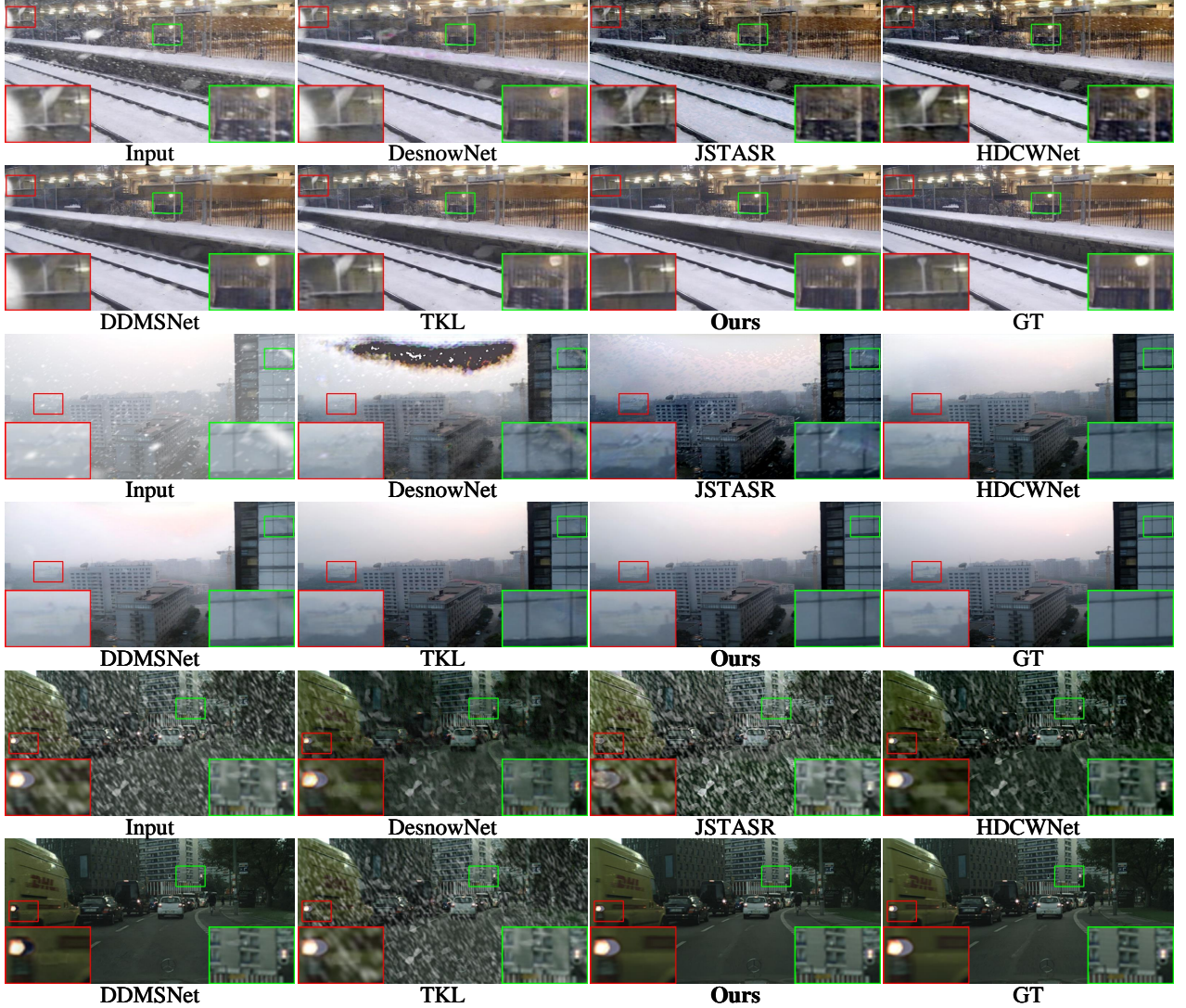


Fig. 8. Visual qualitative comparisons on Snow100K, CSD and SnowCityScapes.

Perceptual Loss  $L_{\text{per}}$  of VGG19 [36] and Edge Loss  $L_{\text{edge}}$ . Edge Loss can be expressed as:

$$L_{\text{edge}} = \frac{1}{N} \sum_{i=1}^N \sqrt{\|\Delta(I_{\text{pred}}) - \Delta(I_{\text{clean}})\|^2 + \varepsilon^2}, \quad (12)$$

where  $\varepsilon=10^{-5}$  represents hyper-parameter constant. The total optimization goal can be expressed as:

$$\mathcal{L}_{\text{MQFormer}} = \mathcal{L}_{\text{char}} + \lambda_1 * \mathcal{L}_{\text{per}} + \lambda_2 * \mathcal{L}_{\text{edge}}, \quad (13)$$

where  $\lambda_1=0.1$  and  $\lambda_2=0.05$  are the hyper-parameter weight between different losses.

## V. EXPERIMENTS AND ANALYSIS

### A. Datasets and Evaluation

1) *Synthetic Datasets*: To better evaluate snow removal performance of our network, we run it on all available synthetic snow removal datasets. They contain Snow100K [9], SRSS [11], CSD [12], SnowKITTI2012 [13] and SnowCityScapes [13]. Note that Snow100K is the first snow removal dataset,

which contains 50000 images in both training set and testing set. SRSS exploits the veiling effect in dataset, which contains 12000 images. CSD introduces snow streaks after SRSS, which contains 8000 images in training set and 2000 images in testing set. Besides, SnowKITTI2012 and SnowCityScapes are street view snow removal datasets. SnowKITTI2012 contains 4500 images in training set and 3000 images in testing set. SnowCityScapes contains 6000 images in training set and testing set. Since snow scenarios are very different for each dataset, multiple datasets allow for a more comprehensive assessment of snow removal methods.

2) *Real-world Dataset*: We employ the Snow100K real-world dataset to verify the generalization ability of the algorithm in the real-world scenarios. This real-world dataset are provided by [9] and consists of 1329 images, which has rich real-world scenarios. Hence we use it to evaluate different methods.

3) *Evaluation*: Each dataset consists of a different number of images. As shown in Table I, we randomly select a specific number of images from each synthetic dataset for training set.



Fig. 9. Visual qualitative comparisons on the real-world images.

TABLE I  
QUANTITATIVE RESULTS EVALUATIONS ON SYNTHETIC DATASETS.

Dataset (testset: 1200)	IQA	DesnowNet (TIP'18)	JSTASR (ECCV'20)	HDCWNet (ICCV'21)	DDMSNet (TIP'21)	TKL (CVPR'22)	Ours
Snow100K (trainset: 10000)	PSNR( $\uparrow$ ) / SSIM( $\uparrow$ ) MAE( $\downarrow$ ) / LPIPS( $\downarrow$ )	23.125/0.788 100.387/0.257	18.648/0.554 129.854/0.437	18.188/0.561 164.356/0.406	<b>29.058/0.891</b> 168.364/ <b>0.103</b>	28.098/0.851 <b>98.232/0.140</b>	<b>31.883/0.917</b> <b>93.999/0.085</b>
SRRS (trainset: 8000)	PSNR( $\uparrow$ ) / SSIM( $\uparrow$ ) MAE( $\downarrow$ ) / LPIPS( $\downarrow$ )	21.307/0.835 119.795/0.290	21.593/0.770 178.618/0.245	25.148/0.893 140.252/0.103	<b>25.967/0.932</b> 136.799/ <b>0.058</b>	25.718/0.909 <b>97.407/0.082</b>	<b>31.040/0.964</b> <b>119.230/0.025</b>
CSD (trainset: 8000)	PSNR( $\uparrow$ ) / SSIM( $\uparrow$ ) MAE( $\downarrow$ ) / LPIPS( $\downarrow$ )	20.632/0.777 152.851/0.309	20.628/0.705 193.095/0.410	28.669/0.892 131.587/0.118	24.976/0.905 130.517/0.084	<b>30.122/0.933</b> <b>123.973/0.058</b>	<b>32.643/0.963</b> <b>121.900/0.029</b>
SnowKITTI2012 (trainset: 4500)	PSNR( $\uparrow$ ) / SSIM( $\uparrow$ ) MAE( $\downarrow$ ) / LPIPS( $\downarrow$ )	16.487/0.682 <b>96.785</b> /0.353	18.470/0.532 143.152/0.407	20.085/0.575 166.774/0.329	<b>30.520/0.934</b> 112.250/ <b>0.053</b>	22.863/0.756 110.321/0.221	<b>33.145/0.959</b> <b>81.847/0.051</b>
SnowCityScapes (trainset: 6000)	PSNR( $\uparrow$ ) / SSIM( $\uparrow$ ) MAE( $\downarrow$ ) / LPIPS( $\downarrow$ )	21.020/0.705 <b>79.821</b> /0.343	19.047/0.550 129.134/0.419	20.385/0.651 190.366/0.310	<b>33.371/0.956</b> 105.535/ <b>0.031</b>	24.412/0.804 162.100/0.208	<b>39.172/0.984</b> <b>67.639/0.010</b>
Parameters(million)		26.151	83.347	<b>18.958</b>	229.454	28.712	<b>2.181</b>
Runtime(s)		2.992	0.356	0.141	0.554	<b>0.051</b>	<b>0.042</b>

As for evaluations, we randomly select 1200 images from each synthetic dataset for compared methods.

4) *Compared Methods*: We compare our method with state-of-the-art deep-learning-based snow removal methods using publicly available codes released by the authors, including DesnowNet [9] (TIP'18), JSTASR [11] (ECCV'20), HDWCNet [12] (ICCV'21), DDMSNet [13] (TIP'21) and TKL [23] (CVPR'22). We use selected training sets, testing sets and four referenced metrics to evaluate these methods, including the Peak Signal to Noise Ratio (PSNR) [37], Structural Similarity Index (SSIM) [38], Mean Absolute Error (MAE) and Learned

Perceptual Image Patch Similarity (LPIPS) [39].

#### B. Implementation Details

Our proposed LMQFormer is trained in two steps. Firstly, Laplace-VQVAE is optimized by Adam and trained for 100 epochs. Secondly, we freeze the weight of Laplace-VQVAE to train LMQFormer. It is optimized by AdamW and trained for 400 epochs. In addition, all sub-networks are trained on randomly cropped  $256 \times 256$  patches with data augmentation of randomly horizontal and vertical flips. The validation dataset is cropped to  $256 \times 256$  in the center. Two learning rates are



Fig. 10. Quality results of different modules. (b) represents H-En w/o Mask; (c) represents P-En w/o Mask; (e) represents P-En + MQTM w/o Mask; (f) represents Ours.

TABLE II  
QUANTITATIVE RESULTS OF DIFFERENT MODULES.

Configurations	H-En w/o Mask	P-En w/o Mask	P-En + M C w/o Mask	P-En + M C w/ Mask (Ours)
PSNR( $\uparrow$ )	27.771	28.745	28.371	<b>29.014</b>
SSIM( $\uparrow$ )	0.895	0.923	0.919	<b>0.931</b>

steadily decreased from the initial learning rate of  $2 \times 10^{-4}$  to  $1 \times 10^{-6}$  using the cosine annealing algorithm. All experiments are performed on a server equipped with four NVIDIA RTX TITAN X GPU with 12GB GPU memory, Linux and PyTorch.

### C. Comparison Results

1) *Quantitative Results on Synthetic Dataset*: From the results of Table I, we can observe that our method achieves the state-of-the-art in all synthetic datasets. For instance, the PSNR of our method is 10.0% higher than the 2nd-best method on Snow100K dataset. On other synthetic datasets, our method also shows strong performance. Our method has only 2.181M parameters, which is only 11.5% of the 2nd best method. Meanwhile, the runtime of our method is only 0.042s, which is 1.21 times faster than the 2nd best method and 71.24 times faster than the lowest method. In summary, these extensive experimental results show the superiority of our proposed method on synthetic datasets.

2) *Qualitative Results on Synthetic Dataset*: Fig. 8 shows the comparison results of all synthetic snow removal datasets. From the results, we can observe that DesnowNet and JSTASR have less image restoration effect and seriously damage the original snowy image. Meanwhile, DDMSNet loses some color and clarity in details. HDCWNet and TKL preserve repairing traces in details. Compared with those methods, the images recovered by our proposed method are not only clean and intact but also preserve better details. The quality results indicate that our method could generate better quality images.

3) *Comparison on Real-World Dataset*: Fig. 9 shows the effects of removing snow in the real-world. We compare magnified images of local details. The quality results show that other snow removal methods lose details and have poor repair

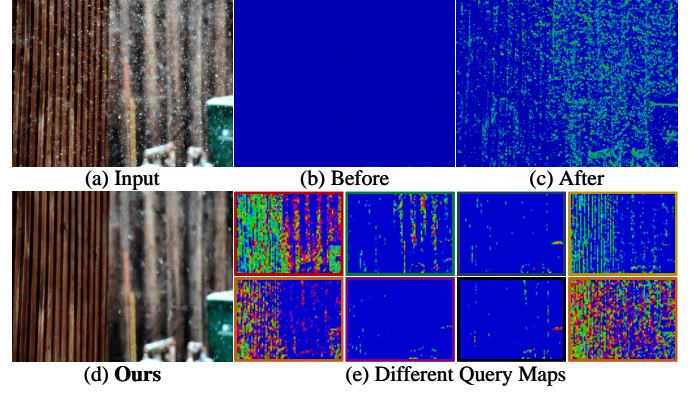


Fig. 11. Visualization of the feature maps.

TABLE III  
QUANTITATIVE RESULTS OF DIFFERENT QUERY NUMBER.  
Q REPRESENTS QUERY NUMBER.

Configurations	4 Q	16 Q	Original Q	8 Q (Ours)
PSNR( $\uparrow$ )	28.767	28.708	28.823	<b>29.014</b>
SSIM( $\uparrow$ )	0.924	0.918	0.924	<b>0.931</b>

effects, which do not work well in the real-world scenarios. In contrast, our algorithm has the best snow removal effect in all cases, with almost no repairing traces in the details. It confirms the excellent generalization performance of our proposed algorithm in the real-world.

### D. Ablation Studies

We explore the contributions of different modules and query number in our proposed method. Evaluation is performed on Snow100K dataset with our method trained for  $2 \times 10^5$  iterations.

1) *Contributions of Different Modules*: Our proposed network consists of three parts: parallel encoders, lightweight modules and mask prior. Specifically, we design parallel encoders to learn features of different dimensions. MQTM and CACM are the main lightweight modules. Meanwhile, mask prior is also an important input feature of our model. We list the following configurations:

**H-En w/o Mask**: Hybrid encoder without the coarse mask as prior knowledge. The encoder has the same architecture as hybrid decoder.

**P-En w/o Mask**: Parallel encoders without the coarse mask as prior knowledge. They are transformer encoder and convolutional encoder.

**P-En + M C w/o Mask**: Parallel encoders without the coarse mask as prior knowledge. MQTM replaces the original vision transformer modules [40]. CACM is added to network.

**P-En + M C w/ Mask (Ours)**: Complete network architecture with the coarse mask as prior knowledge.

From the results of Table II, we can observe that each design has made a contribution to performance. Quality results are shown in Fig. 10. The feature maps before and after MQTM are shown in Fig. 11(b)(c).

2) *Contributions of Different Query Number*: We explore the contributions of different query number. Specifically, we set query number to 4, 16, original number and 8 (Ours). From the results of Table III, we observe a slight performance improvement with a smaller query number. Hence, we set it to 8 in our network. As shown in Fig. 11(e), each query has learned concentrate feature maps, which confirms our main concept of treating Query as a specific number of mask filters.

## VI. CONCLUSION

Snow removal task is critical in computer vision under snowy weather due to the distinct visual appearances and feature distributions of snow. In this paper, we propose a lightweight but high-efficient snow removal network called LMQFormer. It consists of a Laplace-VQVAE sub-network to reduce redundant information entropy with the coarse mask and an MQFormer sub-network to recover clean images without repairing traces. We propose a mask query transformer module to concentrate attention to snow areas. Experimental results show that our proposed LMQFormer achieves superior performance on all existing snow removal datasets, whilst its parameters is significantly reduced compared with its peers.

## REFERENCES

- [1] C. Chen and H. Li, “Robust representation learning with feedback for single image deraining,” in *Proc. IEEE Conf. Comput. Vis. Pattern Recognit.*, 2021, pp. 7742–7751.
- [2] Y. Yang, C. Wang, R. Liu, L. Zhang, X. Guo, and D. Tao, “Self-augmented unpaired image dehazing via density and depth decomposition,” in *Proc. IEEE Conf. Comput. Vis. Pattern Recognit.*, 2022, pp. 2037–2046.
- [3] L. Ma, T. Ma, R. Liu, X. Fan, and Z. Luo, “Toward fast, flexible, and robust low-light image enhancement,” in *Proc. IEEE Conf. Comput. Vis. Pattern Recognit.*, 2022, pp. 5637–5646.
- [4] W. Zhang, P. Zhuang, H.-H. Sun, G. Li, S. Kwong, and C. Li, “Underwater image enhancement via minimal color loss and locally adaptive contrast enhancement,” *IEEE Trans. Image Process.*, vol. 31, pp. 3997–4010, 2022.
- [5] V. V. Voronin, E. Semenishchev, M. Zhdanova, R. Sizyakin, and A. Zelenetskii, “Rain and snow removal using multi-guided filter and anisotropic gradient in the quaternion framework,” in *Proc. SPIE Int. Soc. Opt. Eng.*, 2019.
- [6] Y. Wang, S. Liu, C. Chen, and B. Zeng, “A hierarchical approach for rain or snow removing in a single color image,” *IEEE Trans. Image Process.*, pp. 3936–3950, 2017.
- [7] S.-C. Pei, Y.-T. Tsai, and C.-Y. Lee, “Removing rain and snow in a single image using saturation and visibility features,” in *IEEE Int. Conf. Multimed. Expo Workshops*, 2014, pp. 1–6.
- [8] J. Bossu, N. Hautière, and J. P. Tarel, “Rain or snow detection in image sequences through use of a histogram of orientation of streaks,” *Int. J. Comput. Vis.*, vol. 93, no. 3, pp. 348–367, 2011.
- [9] Y.-F. Liu, D.-W. Jaw, S.-C. Huang, and J.-N. Hwang, “Desnownet: Context-aware deep network for snow removal,” *IEEE Trans. Image Process.*, vol. 27, no. 6, pp. 3064–3073, 2018.
- [10] Z. Li, J. Zhang, Z. Fang, B. Huang, X. Jiang, Y. Gao, and J.-N. Hwang, “Single image snow removal via composition generative adversarial networks,” *IEEE Access*, vol. 7, pp. 25 016–25 025, 2019.
- [11] W.-T. Chen, H.-Y. Fang, J.-J. Ding, C.-C. Tsai, and S.-Y. Kuo, “Jstar: Joint size and transparency-aware snow removal algorithm based on modified partial convolution and veiling effect removal,” in *Proc. Eur. Conf. Comput. Vis.* Springer, 2020, pp. 754–770.
- [12] W.-T. Chen, H.-Y. Fang, C.-L. Hsieh, C.-C. Tsai, I. Chen, J.-J. Ding, S.-Y. Kuo *et al.*, “All snow removed: Single image desnowing algorithm using hierarchical dual-tree complex wavelet representation and contradict channel loss,” in *Proc. IEEE Int. Conf. Comput. Vis.*, 2021, pp. 4196–4205.
- [13] K. Zhang, R. Li, Y. Yu, W. Luo, and C. Li, “Deep dense multi-scale network for snow removal using semantic and depth priors,” *IEEE Trans. Image Process.*, vol. 30, pp. 7419–7431, 2021.
- [14] Z. Yue, J. Xie, Q. Zhao, and D. Meng, “Semi-supervised video deraining with dynamical rain generator,” in *Proc. IEEE Conf. Comput. Vis. Pattern Recognit.*, 2021, pp. 642–652.
- [15] K. Jiang, Z. Wang, P. Yi, C. Chen, Z. Wang, X. Wang, J. Jiang, and C.-W. Lin, “Rain-free and residue hand-in-hand: A progressive coupled network for real-time image deraining,” *IEEE Trans. Image Process.*, vol. 30, pp. 7404–7418, 2021.
- [16] L. Cai, S.-Y. Li, D. Ren, and P. Wang, “Dual recursive network for fast image deraining,” in *Proc. Int. Conf. Image Process. ICIP*. IEEE, 2019, pp. 2756–2760.
- [17] H. Wang, Q. Xie, Q. Zhao, and D. Meng, “A model-driven deep neural network for single image rain removal,” in *Proc. IEEE Conf. Comput. Vis. Pattern Recognit.*, 2020, pp. 3103–3112.
- [18] X. Fu, J. Huang, D. Zeng, Y. Huang, X. Ding, and J. Paisley, “Removing rain from single images via a deep detail network,” in *Proc. IEEE Conf. Comput. Vis. Pattern Recognit.*, 2017, pp. 3855–3863.
- [19] W. Yang, R. T. Tan, J. Feng, J. Liu, Z. Guo, and S. Yan, “Deep joint rain detection and removal from a single image,” in *Proc. IEEE Conf. Comput. Vis. Pattern Recognit.*, 2017, pp. 1357–1366.
- [20] X. Zheng, Y. Liao, W. Guo, X. Fu, and X. Ding, “Single-image-based rain and snow removal using multi-guided filter,” in *Lect. Notes Comput. Sci.* Springer, 2013, pp. 258–265.
- [21] D. Rajderkar and P. Mohod, “Removing snow from an image via image decomposition,” in *IEEE Int. Conf. Emerg. Trends Comput., Commun. Nanotechnology, ICE-CCN*, 2013, pp. 576–579.
- [22] R. Li, R. T. Tan, and L.-F. Cheong, “All in one bad weather removal using architectural search,” in *Proc. IEEE Conf. Comput. Vis. Pattern Recognit.*, 2020, pp. 3175–3185.
- [23] W.-T. Chen, Z.-K. Huang, C.-C. Tsai, H.-H. Yang, J.-J. Ding, and S.-Y. Kuo, “Learning multiple adverse weather removal via two-stage knowledge learning and multi-contrastive regularization: Toward a unified model,” in *Proc. IEEE Conf. Comput. Vis. Pattern Recognit.*, 2022, pp. 17 653–17 662.
- [24] X. Fu, Q. Qi, Z.-J. Zha, X. Ding, F. Wu, and J. Paisley, “Successive graph convolutional network for image de-raining,” *Int. J. Comput. Vis.*, vol. 129, no. 5, pp. 1691–1711, 2021.
- [25] J. Li, X. Feng, and Z. Hua, “Low-light image enhancement via progressive-recursive network,” *IEEE Trans. Circuits Syst. Video Technol.*, vol. 31, no. 11, pp. 4227–4240, 2021.
- [26] J. Zhou, D. Zhang, and W. Zhang, “Underwater image enhancement method via multi-feature prior fusion,” *Appl. Intell.*, pp. 1–23, 2022.
- [27] W. Zou, Y. Wang, X. Fu, and Y. Cao, “Dreaming to prune image deraining networks,” in *Proc. IEEE Conf. Comput. Vis. Pattern Recognit.*, June 2022, pp. 6023–6032.
- [28] K. Zhang, D. Li, W. Luo, W. Ren, and W. Liu, “Enhanced spatio-temporal interaction learning for video deraining: A faster and better framework,” *IEEE Trans. Pattern Anal. Mach. Intell.*, 2022.
- [29] H. Wu, Y. Qu, S. Lin, J. Zhou, R. Qiao, Z. Zhang, Y. Xie, and L. Ma, “Contrastive learning for compact single image dehazing,” in *Proc. IEEE Conf. Comput. Vis. Pattern Recognit.*, 2021, pp. 10 551–10 560.
- [30] Y. Wang, R. Wan, W. Yang, H. Li, L.-P. Chau, and A. Kot, “Low-light image enhancement with normalizing flow,” in *Proc. AAAI Conf. Artif. Intell.*, vol. 36, no. 3, 2022, pp. 2604–2612.
- [31] N. Jiang, W. Chen, Y. Lin, T. Zhao, and C.-W. Lin, “Underwater image enhancement with lightweight cascaded network,” *IEEE Trans. Multimedia*, 2021.
- [32] A. Van Den Oord, O. Vinyals *et al.*, “Neural discrete representation learning,” *Proc. Annu. Conf. Neural Inf. Process. Syst.*, vol. 30, 2017.
- [33] D. P. Kingma and M. Welling, “Auto-encoding variational bayes,” *Int. Conf. Learn. Represent., ICLR - Conf. Track Proc.*, 2014.
- [34] Z. Liu, H. Mao, C.-Y. Wu, C. Feichtenhofer, T. Darrell, and S. Xie, “A convnet for the 2020s,” in *Proc. IEEE Conf. Comput. Vis. Pattern Recognit.*, 2022, pp. 11 976–11 986.
- [35] W.-S. Lai, J.-B. Huang, N. Ahuja, and M.-H. Yang, “Fast and accurate image super-resolution with deep laplacian pyramid networks,” *IEEE Trans. Pattern Anal. Mach. Intell.*, vol. 41, no. 11, pp. 2599–2613, 2018.
- [36] J. Justin, A. Alexandre, and F.-F. Li, “Perceptual losses for real-time style transfer and super-resolution,” in *Proc. Eur. Conf. Comput. Vis.* Springer, 2016, pp. 694–711.
- [37] H. R. Sheikh, M. F. Sabir, and A. C. Bovik, “A statistical evaluation of recent full reference image quality assessment algorithms,” *IEEE Trans. Image Process.*, vol. 15, no. 11, pp. 3440–3451, 2006.
- [38] W. Zhou, A. C. Bovik, H. R. Sheikh, and E. P. Simoncelli, “Image quality assessment: from error visibility to structural similarity,” *IEEE Trans. Image Process.*, vol. 13, no. 4, 2004.

- [39] R. Zhang, P. Isola, A. A. Efros, E. Shechtman, and O. Wang, “The unreasonable effectiveness of deep features as a perceptual metric,” in *Proc. IEEE Conf. Comput. Vis. Pattern Recognit.*, 2018, pp. 586–595.
- [40] A. Dosovitskiy, L. Beyer, A. Kolesnikov, D. Weissenborn, X. Zhai, T. Unterthiner, M. Dehghani, M. Minderer, G. Heigold, S. Gelly *et al.*, “An image is worth 16x16 words: Transformers for image recognition at scale,” *arXiv preprint arXiv:2010.11929*, 2020.